Modelling the impact of operating mode and electron transfer mechanism in microbial fuel cells with two-species anodic biofilm

Ziming Yang[a], Aidong Yang[a]*

[a] *Department of Engineering Science, University of Oxford, Parks Road, Oxford, OX1 3PJ, United Kingdom*

* *Corresponding author. E-mail address: aidong.yang@eng.ox.ac.uk*

Abstract

In this study, mathematical models are developed for a Microbial Fuel Cell (MFC) with a 'fermenter-Electrochemically Active Bacteria (EAB)' type, two-species biofilm, governed by Mediator-Based Extracellular Electron Transfer (MET) or Direct Conduction-Based Extracellular Electron Transfer (DET), and operating under a batch or continuous mode. Numerical simulations have been carried out to test the impact of a range of physical and biochemical parameters on biofilm composition and current generation.

The results reveal the contrast between two operating modes, caused by the difference in the length of time available and in the substrate supply for the evolution of the biofilm, and the contrast between systems governed by MET and DET, arising primarily from the difference between the role of the mediator and that of the electrical potential played in the two systems, respectively. Many observations, including several counter-intuitive occasions, stem from the trade-offs between the impacts of the process parameters on bioelectrochemical kinetics, mass transfer, and electrical resistance. The simulation results also predict the existence of optimal parameter settings in various cases for the purpose of electricity generation. These findings provide potentially useful insights to guide the design and operation of MFCs or other types of bioelectrochemical devices that employ multi-species biofilms.

Keywords

Microbial fuel cell; Modelling; Two-species biofilm; Extracellular electron transfer; Biofilm composition; Power generation

1. Introduction

In recent decades, climate change and other environmental issues associated with the use of fossil fuels make it urgent to explore green and renewable energy options. Bioelectrochemical Systems (BESs), which generate electricity or valuable products [1–3] (such as hydrogen [4,5], hydrogen peroxide [6] and methane [7,8]) from low-cost substrates by the use of microorganisms, hold great potential in a wide range of energy, environmental and other biological applications. As an important example of BESs, Microbial Fuel Cells (MFCs) are able to generate electricity from microbially catalysed anodic oxidation processes in the absence of conventional metal catalysts, with potential applications in several areas such as energy recovery, water purification, and biosensors for oxygen and pollutants [2,9,10]

MFCs rely on the biofilm attached on the anode to harvest energy and harness electrons from substrate. The microorganisms that are able to oxidize substrates and achieve Extracellular Electron Transfer (EET) are often referred to as Electrochemically Active Bacteria (EAB). To date, two prevailing types of EET have been considered, namely Mediator-Based Extracellular Electron Transfer (MET) and Direct Conduction-Based Extracellular Electron Transfer (DET). MET relies on soluble mediators as electron shuttles to convey electrons from bacteria cells to the anode surface. Oxidised mediators act as the primary Electron Acceptor (EA) to extract electrons from substrate, and reduced mediators subsequently diffuse to the anode surface, where electrons are released and the mediator is re-oxidised. In DET, electrons are supplied to the anode directly via exchange with conductive biofilm in this type [11-13]

While a single species of EAB can be capable of completing the conversion of certain types of substrate to electrons on its own, it has been shown that synergy may exist in a multispecies biofilm compared to pure culture which enhances substrate conversion, electron transfer and power output [9,14-16]. For example, the 'fermenter-EAB' community of *Shewanella oneidensis* (*S. oneidensis*) and *Escherichia coli* (*E. coli*) was investigated, with the latter acting as a fermenter to convert the primary substrate (glucose) into what the former (acting as the EAB) could utilize [17,18]. More recently, a microbial consortium comprising *S. oneidensis* MR-1 and *Bacillus subtilis* RH33 was utilised, in which the latter, nonelectrogenic microbe produced a high amount of mediators (riboflavin) to boost bioelectricity generation of the former, which is an EAB [16]. Both of the two studies found that the maximum voltage output,

substrate utilization and electron transfer efficiency of the mixture consortia were higher than the pure culture. In addition, it was reported by several studies that a synthesised mixture community was capable to sustain high diversity by avoiding one species dominating and to resist external environmental disturbances, hence improving the overall stability of the system [16, 19].

Up to now, most studies on the multispecies BESs (and MFCs in particular) are of a nature of experimental exploration [16-18,20]. On mathematical modelling, only a handful of modelling studies address multispecies systems. An earlier work simulated anodic biofilms with Anaerobic Digestion (AD), where the microbial community involved EAB and the typical microbial populations of AD, with MET as the modelled EET mechanism. The dynamic evolution of several variables (solute concentration in the bulk liquid, distribution of current density and biomass on the anode) were evaluated and the effect of external resistance was considered, which however did not focus on the interplay between various mechanisms [21]. Later, the model of multispecies AD biofilm was extended to include further details such as the pH variation in the liquid flow at the anodic chamber, yet without revealing the spatial distribution of multiple species in the biofilm [22].A very recent study presented the modelling of four microbial groups in a bioanode which carried out fermentation, electroactivity and methanogenesis, with DET as the assumed EET mechanism [23]. All these existing modelling studies are yet to be extended to support further systematic analysis of multi-species bioanodes, particularly on the evolution and stability of the microbial communities in anodic biofilms in connection with various internal mechanisms and operating conditions.

In this work, new insights are sought with respect to (i) the spatial distribution and dynamics of a multi-species biofilm hosting bioelectrochemical processes, and (ii) their impact on electricity generation in a MFC. Adopting a relatively simple, 1-D biofilm model and a two-species “fermenter-EAB” consortium, the focus of this work is to analyse in detail the change in the composition of the biofilm resulting from the interplay between electrochemical kinetics, mass transport and EET mechanisms, under the influence of (i) biofilm characteristics such as maximum thickness, conductivity, and seeding ratio of the initial populations, (ii) operating mode, i.e. batch or continuous, and (iii) operating settings such as substrate supply,

dilution rate and external electrical resistance. The purpose of this study is to develop an understanding of the impact of these key factors and their trade-offs, hence offering insights for the future engineering of multi-species biofilms in MFCs and other similar BESs.

2. Model description

The constructed model focuses on the anode chamber of a MFC operating with an external electrical resistance. The anode chamber comprises an electrode with biofilm attachment and a bulk liquid phase in which the electrode is embedded. The biofilm is based on a two-species community, with a fermenter to convert a primary substrate to an intermediate substrate to feed an EAB. The biofilm is assumed to only grow in the x-axis direction which is perpendicular to the impenetrable anode surface, i.e. the direction in which the biofilm heterogeneity is typically dominant [24]. The biofilm inner surface, i.e. that next to the supporting electrode base, is located at $x = 0$; the interface with the bulk liquid phase (where x = biofilm thickness) is referred to as the outer surface. The whole model for the anode chamber is divided into three sub-models: Electrode, Biofilm and Bulk Liquid sub-models. Their formulations with two different operating modes (batch and continuous) and two EET mechanisms (MET and DET) are presented below. In "fermenter-EAB" type of multispecies system, the soluble components consist of primary substrate (i.e. the substrate directly added to the MFC), intermediate substrate (i.e. the product generated by the fermenter to feed the EAB) and two forms of mediator (i.e. oxidised and reduced).

2.1. Electrode sub-models

2.1.1. MET-based model

The current generation via the MET pathway relies on the conversion of the two forms of a mediator at the anode surface. This reversible chemical process is depicted as:

$$C_{Mr,F}|_{x=0} \underset{r_{red}}{\overset{r_{ox}}{\leftrightarrows}} C_{Mo,F}|_{x=0} + ne^-$$

$C_{Mr,F}|_{x=0}$ and $C_{Mo,F}|_{x=0}$ represent the concentrations of the reduced and oxidized forms of the mediator (Mr and Mo) at the anode surface, respectively. For a given reversible redox

reaction and given concentrations of the involved chemical species, the anode potential (V_a) (which determines the over potential) is the decisive factor of the reaction direction. A higher (lower) potential increases the rate of the oxidation (reduction) process per unit electrode surface area, r_{ox} (r_{red}). The oxidation and reduction rates of the mediator at the anode surface, are governed by the Butler-Volmer kinetics as commonly adopted in MFC models (e.g. [11,12,25,26]):

$$r_{ox} = k_a C_{Mr,F}|_{x=0} \exp\left(\frac{(1-\beta)nF}{RT} V_a\right) \quad (1)$$

$$r_{red} = k_c C_{Mo,F}|_{x=0} exp\left(\frac{-\beta nF}{RT} V_a\right) \quad (2)$$

where k_a, k_c are the oxidation and reduction rate constants, respectively; β is the transfer coefficient, representing the fraction of the anode potential that favours the reduction reaction, r_{red}; n is the number of electrons transferred per redox mediator reaction; T is the operating temperature. Note that resolving V_a involves Eq. (8) which is to introduce later. The net redox reaction rate, r_E equals to ($r_{ox} - r_{red}$), and the current density, i_M is:

$$i_M = nFr_E \quad (3)$$

where F is the Faraday constant.

2.1.2. DET-based model

With DET, electrons generated from the (intermediate) substrate oxidation process (assuming no endogenous respiration) are conducted to the anode surface through the biofilm matrix with an assumed constant conductivity, k. Similar to enzymatic reactions, electron transfer via DET is considered as an irreversible process, meaning electrons only have the oxidation current (i.e. electrons flow towards anode) and cannot be sent back to the cells due to irreversibility of the microbial metabolic processes [12,13,27]

The change in current (i_C) in the biofilm matrix is caused by the production of electrons via DET [13]:

$$\frac{\partial i_C}{\partial x} = -FR_C \quad (4)$$

where R_C is the electron generation rate via DET. R_C is obtained based on electron balance [12]:

$$R_C = \frac{yfX_{EAB,F}\mu_{EAB,C}}{Y_{EAB/I}} \tag{5}$$

where y is the electron equivalence of EAB's substrate; f is the fraction of electrons recoverable from EAB's substrate for current generation; $Y_{EAB/I}$ is the yield of EAB on its substrate; $X_{EAB,F}$ and $\mu_{EAB,C}$ are the EAB's biomass concentration in the biofilm and the specific growth rate associated with the DET mechanism, respectively. $X_{EAB,F}$ and $\mu_{EAB,C}$ will be described further in the following sections.

Ohm's law defines the relationship between the anode potential, V_a and current density, corresponding to an assumed electron hopping process within the biofilm adjacent to the anode [13,28]

$$k\frac{\partial V_a}{\partial x} + i_C = 0 \tag{6}$$

Collectively, Eqs. (4) to (6) can lead to the governing Eq. (7) used for simulating potential changes in the anodic biofilm:

$$k\frac{\partial^2 V_a}{\partial x^2} = \frac{FyfX_{EAB,F}\mu_{EAB,C}}{Y_{EAB/I}} \tag{7}$$

The following equation, which is also derived from Ohm's law acts as the boundary condition at the biofilm inner surface to solve Eq. (7) [29]:

$$V_a = V_c - iA_E(R_{int} + R_{ext}) \tag{8}$$

where V_c is the cathode potential; A_E is the electrode surface area; R_{int} and R_{ext} represent the internal and external resistance, respectively. Note that Eq. (8) is also used in the MET-based model for resolving V_a. A non-flux boundary condition is adopted for Eq. (7) at the biofilm outer surface. Focusing on the simulation of the anode chamber, V_c is assumed to be fixed to a specific value while V_a is predicted [26].

2.2. Biofilm sub-model

2.2.1. *Mass balance of soluble components*

In the anode chamber considered in this work, soluble components are present in the biofilm (modelled here) and in the bulk liquid phase (modelled in Section 2.3). These components include the primary substrate, the intermediate substrate and, in the case of MET, the oxidised form and the reduced form of the mediator. Concentrations of soluble components in the biofilm are a function of time and location. Mass balance for any soluble component can be expressed as:

$$\frac{\partial C_{S,F}}{\partial t} = \frac{\partial}{\partial x}\left(D_{S,F}\frac{\partial C_{S,F}}{\partial x}\right) - R_{S,F} \tag{9}$$

where $C_{S,F}$ is the concentration of a soluble component in the biofilm; $D_{S,F}$ is the diffusion coefficient for the soluble component in the biofilm; $R_{S,F}$ denotes the net consumption rate of the soluble component. Eq. (9) states that the concentration of a dissolved component in the biofilm changes in response to the molecular diffusion (first term on the right hand side) and reactions (second term on the right hand side) in the biofilm.

Based on Fick's first law and continuity of the flux at biofilm/bulk liquid interface, the flux of a soluble component across the interface, $J_{S,F}$ (defined as per unit cross-sectional area of the entire biofilm) is given below, assuming a constant concentration gradient in the diffusion layer on the bulk liquid side adjacent to the biofilm outer surface (where $x = L_F$, the biofilm thickness):

$$J_{S,F} = -D_{S,F}\frac{\partial C_{S,F}}{\partial x}|_{x=L_F} = \frac{D_{S,B}}{L_D}(C_{S,B}\varepsilon - C_{S,F}|_{x=L_F}) \tag{10}$$

where $D_{S,B}$ is the diffusion coefficient in the bulk liquid; L_D is the diffusion layer thickness; ε is the porosity of the biofilm, introduced into the equation to account for the nature of the concentrations in the biofilm being per unit volume of the entire biofilm (i.e. solid matrix plus void space occupied by fluid). Eq. (10) serves as the boundary condition for Eq. (9) at the biofilm outer surface.

At the inner surface of the biofilm, i.e. the anode surface, the following mass balance applies [26]:

$$D_{S,F}\frac{\partial C_{S,F}}{\partial x}|_{x=0} + r_{S,E} = 0 \quad (11)$$

where $r_{S,E}$ is the production rate of the soluble component per unit surface area. For components not involved in reactions at this surface (i.e. primary and intermediate substrates), the consumption rate becomes zero.

2.2.2. Mass balance of biomass

Mass balance of the biomass of each microbial species considers biomass production and advective movement due to biofilm growth [13,30]:

$$\frac{\partial X_F}{\partial t} + \frac{\partial (vX_F)}{\partial x} = R_{X,F} \quad (12)$$

where X_F is the biomass concentration of one microbial species in the biofilm. v is the advective velocity (i.e. the velocity at which the biofilm grows along the x-axis); $R_{X,F}$ is the net reaction rate of biomass.

As a simplifying assumption, inactivation of biomass is ignored. The advective velocity is modelled as below, with zero flux applied at the anode/biofilm [4,5]:

$$\frac{\partial v}{\partial x} = \frac{\sum R_{X,F}}{\rho_F} \quad (13)$$

where ρ_F is the biofilm biomass density, which is defined as the ratio of dry biomass weight and biofilm volume.

2.2.3. Growth kinetics

Growth of the Fermentative Bacteria (FB) is modelled according to the Monod Equation:

$$\mu_{FB} = \mu_{max,FB}\frac{C_{P,F}}{C_{P,F} + K_P} \quad (14)$$

where μ_{FB} is the specific growth rate; $\mu_{max,FB}$ is the maximum specific growth rate; $C_{P,F}$ is the primary substrate concentration in the biofilm; K_P is the half-saturation constant.

The specific growth rate of the EAB is controlled by both its substrate and the EA. With MET, the oxidised mediator plays the role of EA. During the reaction with the intermediate

substrate that feeds the EAB, the soluble mediator is reduced by capturing electrons from the intermediate substrate and then diffused towards the anode surface, discharging its electrons there and converted (re-generated) to the oxidised form. The rate of EAB's specific growth rate with the MET mechanism, $\mu_{EAB,M}$ can be modelled by the double Monod kinetic equation, which is frequently used to represent the dual limitation [12,13,26,31-34]

$$\mu_{EAB,M} = \mu_{max,EAB} \frac{C_{I,F}}{C_{I,F}+K_I} \frac{C_{Mo,F}}{C_{Mo,F}+K_{Mo}} \quad (15)$$

where K_{Mo} is the half-saturation constant; $\mu_{max,EAB}$ is the maximum specific growth rate; $C_{I,F}$ and $C_{Mo,F}$ represent the concentration of the intermediate substrate and that of the EA (i.e. Mo), respectively; K_I, K_{Mo} are the half-saturation constants corresponding to the intermediate substance and the EA. In the case of DET, the biofilm-modified anode is assumed to be the only EA which accepts the electrons generated by the EAB through the biofilm matrix comprising Extracellular Polymeric Substances (EPS) and biomass [6]. Modifying the double Monod equation and using anode potential, V_a, as the driving force of electrons transfer, the rate of EAB's specific growth rate in DET mechanism $\mu_{EAB,C}$ can be modelled by the Nernst-Monod Equation, commonly adopted in previous modelling work [13,23,27,29]

$$\mu_{EAB,C} = \mu_{max,EAB} \frac{C_{I,F}}{C_{I,F}+K_I} \frac{1}{1+\exp\left(-\frac{F}{R_{ideal}T}(V_a-E_{KA})\right)} \quad (16)$$

where E_{KA} denotes the anode potential corresponding to half-maximum specific growth rate.

The growth of FB leads to the conversion of the primary substrate to the intermediate substrate. The growth of the EAB with either EET mechanism causes the consumption of the intermediate substrate in the biofilm. In the MET case, it also causes the consumption of the oxidised mediator and the production of the reduced mediator. These chemical conversion rates are modelled through links with the growth kinetics via respective yield coefficients (see SI, Section I for details).

2.2.4. Endogenous mediator secretion

Cell proliferation of the *Shewanella* Species was previously shown to be clearly accompanied by the secretion of the mediator in its oxidised form (Mo). Here, the specific Mo secretion rate (μ_{Mo}) is modelled by a Monod-type equation [36]:

$$\mu_{Mo} = \mu_{max,Mo} \frac{C_{I,F}}{C_{I,F} + K_I} \tag{17}$$

where $\mu_{max,Mo}$ represents the maximum specific Mo secretion rate. The abundance of Mo in the anode chamber is determined by the initial concentration of the mediator (which is assumed to be all in the oxidised form) and the endogenous secretion; no external mediator addition is considered. A previous study found that the rate of ATP production for *Shewanella* was 1,000-fold faster than the rate of ATP consumption for Flavin synthesis, which suggests negligible consumption of the substrate by Mo secretion [37]. Therefore, the Mo excretion process is excluded in the mass balance of the intermediate substrate.

2.3. Bulk liquid sub-model

The bulk liquid phase plays a role of supplying nutrients to the biofilm. Through diffusion, other soluble components can also be exchanged between the bulk liquid phase and the biofilm. The bulk liquid compartment is treated as a well-mixed volume. As this work focuses on the biofilm, no planktonic biomass is modelled in the bulk liquid, unless stated otherwise. Moreover, detached biomass from the biofilm is also neglected.

In a batch system, the mass balance of a soluble component in the bulk liquid is described as below:

$$\frac{dC_{S,B}}{dt} = -\frac{1}{V_B} J_{S,F} A_F \tag{18}$$

where $C_{S,B}$ is the concentration of a soluble component in the bulk liquid; A_F is the area of the liquid-biofilm interface, i.e. the cross-sectional area of the biofilm, identical to the anode surface area, A_E.

In a continuous system where the bulk liquid volume is connected with an inlet flow and an outlet flow with the same volumetric flowrate, V_f, the mass balance of a soluble component is written as:

$$\frac{dC_{S,B}}{dt} = -\frac{1}{V_B} J_{S,F} A_F + \frac{V_f}{V_B}(C_{S,in} - C_{S,B}) \tag{19}$$

where $C_{S,in}$ is the concentration of the soluble component in the inlet flow.

2.4. Biofilm thickness

Referring to the advective velocity of the biofilm as introduced earlier in Eq. (13), the biofilm thickness changes as follows:

$$\frac{dL_F}{dt} = v|_{x=L_F} \tag{20}$$

The above equation ignores the detachment loss of biomass from the biofilm at its outer surface, and ceases to be active once the biofilm thickness has reached a pre-defined maximum level. To avoid dealing with the moving outer boundary of the biofilm due to its growth, a converted coordination is constructed by introducing ζ, defined as [13,30]:

$$\zeta = \frac{x}{L_F} \tag{21}$$

This treatment allows the above-mentioned boundary to be fixed at $\zeta = 1$. This conversion requires the previously introduced functions $f(x,t)$ to be converted to $f(\zeta,t)$ in accordance with the following rules in which $\frac{dL_F}{dt}$ is termed as u_L [30]:

$$\frac{\partial f(x,t)}{\partial x} = \frac{1}{L_F}\frac{\partial f(\zeta,t)}{\partial \zeta} \tag{22}$$

$$\frac{\partial f(x,t)}{\partial t} = \frac{\partial f(\zeta,t)}{\partial t} - \frac{\zeta u_L}{L_F}\frac{\partial f(\zeta,t)}{\partial \zeta} \tag{23}$$

Biofilm growth has been modelled in all the simulations of a batch system. For continuous systems, preliminary tests in this work showed that the simulation results were affected to a negligible extent by the inclusion of the phase where the biofilm grows from its initial thickness to its maximum thickness, and this phase also turned to be rather short compared

to the time needed for the system to reach a steady state. Therefore, when a continuous system was simulated, this phase of growth was neglected, and a constant biofilm thickness was applied.

3. Model implementation and application

All constructed models have been implemented in the COMSOL Multiphysics Software (5.3a Version COMSOL Inc., Burlington, MA, USA).

We have applied the models to an anodic biofilm with *S. oneidensis, (as known as* MR1) as the EAB and *E. coli* as the FB. For *S. oneidensis*, the existence of multiple electron transfer pathways including MET and DET has been confirmed by several studies [12,27,38,39]. The same consortium was used in a previously reported experimental study [17], where *E. coli* metabolised glucose to lactate, formate and acetate, and *S. oneidensis* utilised intermediate metabolites to generate and transport electrons. It was suggested that formate was the main substrate for *S. oneidensis*, and EET was assumed to be via MET. It was also suggested that part of the electricity generation was by *E. coli*. In the present theoretical study, we have followed the divide between the roles of the fermenter (only producing the intermediate substrate, not electricity) and the EAB (being the only electricity producer) as presented earlier in Model Description, and have taken formate as the only intermediate substrate to be consumed by the EAB, i.e. *S. oneidensis*. Besides, both EET mechanisms have been simulated. Given the key differences between the experiments reported in [10] and the systems to be simulated in this work, the physical and biochemical parameters were obtained from literature sources with no re-calibration to experimental data, although we have adopted, where information is available and applicable, the design and operational settings reported in [17]. All parameters adopted in our simulation study are listed in Table S1 (see SI, Section II), with items that deserve an explanation being described below.

Because of the presence of biomass, EPS and other abiotic partials or trapped gas bubbles, the effective diffusion coefficients will be reduced. A relative diffusion coefficient, which is defined by the ratio of $D_{S,F}/D_{S,B}$ is used for describing this reduction. All effective diffusion coefficients in bulk liquid and biofilm for soluble components can be determined based on the information from relevant sources (see SI, Section III).

For the mediator, one of the active form of riboflavin, Flavin mononueleotide (FMN) is assumed in this work, which has previously been characterised [12,40,41]. The rate constants of the mediator oxidisation and reduction reactions, k_a and k_c can be determined by the reference exchange current density, $i_{o,ref}$ and the standard mediator redox potential, E^0. The reference exchange current density, $i_{o,ref}$ in the mediator redox reaction is determined by assuming that reactant and oxidant concentrations are $1\ mM$ and the reaction transfer coefficient is 0.5:

$$i_{o,ref} = nF{k_a}^{0.5}{k_c}^{0.5} \tag{24}$$

Furthermore, the equilibrium potential in the reference condition is identical to the standard mediator redox potential. Therefore, according to the Nernst equation, the relationship between the standard mediator redox reaction and the oxidisation and reduction reaction constants can be developed:

$$E^0 = \frac{RT}{nF}\ln\frac{k_c}{k_a} \tag{25}$$

Combining Eqs. (24) and (25), the values of k_a and k_c can be obtained with given values of $i_{o,ref}$ and E^0.

4. Results

In this section, we present and interpret simulation results, to analyse the variation in the predicted biofilm composition and the corresponding power generation performance of the simulated MFC, under batch and continuous operating modes, two different EET mechanisms (MET and DET), and a range of chemical, biological and physical conditions. Note that in all the simulation studies reported here, when different values of a specific parameter are tested, all other parameters retain their default values as given in Table S1 (see SI, Section II), unless stated otherwise. A summary of the key results is provided in Table S3 (a) and (b) (see SI, Section IX) for the batch mode and the continuous mode, respectively.

4.1. Batch mode

Here, we are interested in the impact of the two key initial conditions of a batch run, namely the concentrations of glucose and Mo and the MR1:*E. coli* seeding ratio in the initial biofilm. Besides, the maximum thickness reachable by the biofilm affects the absolute amount of biomass accommodated by the biofilm and the resistance to mass transfer and current. The external electrical resistance, on the other hand, may change the growth condition of the EAB through affecting the anode potential [42]. Therefore, these two parameters are also studied.

4.1.1. The effect of initial concentration of primary substrate (glucose), $C_{P,B,0}$

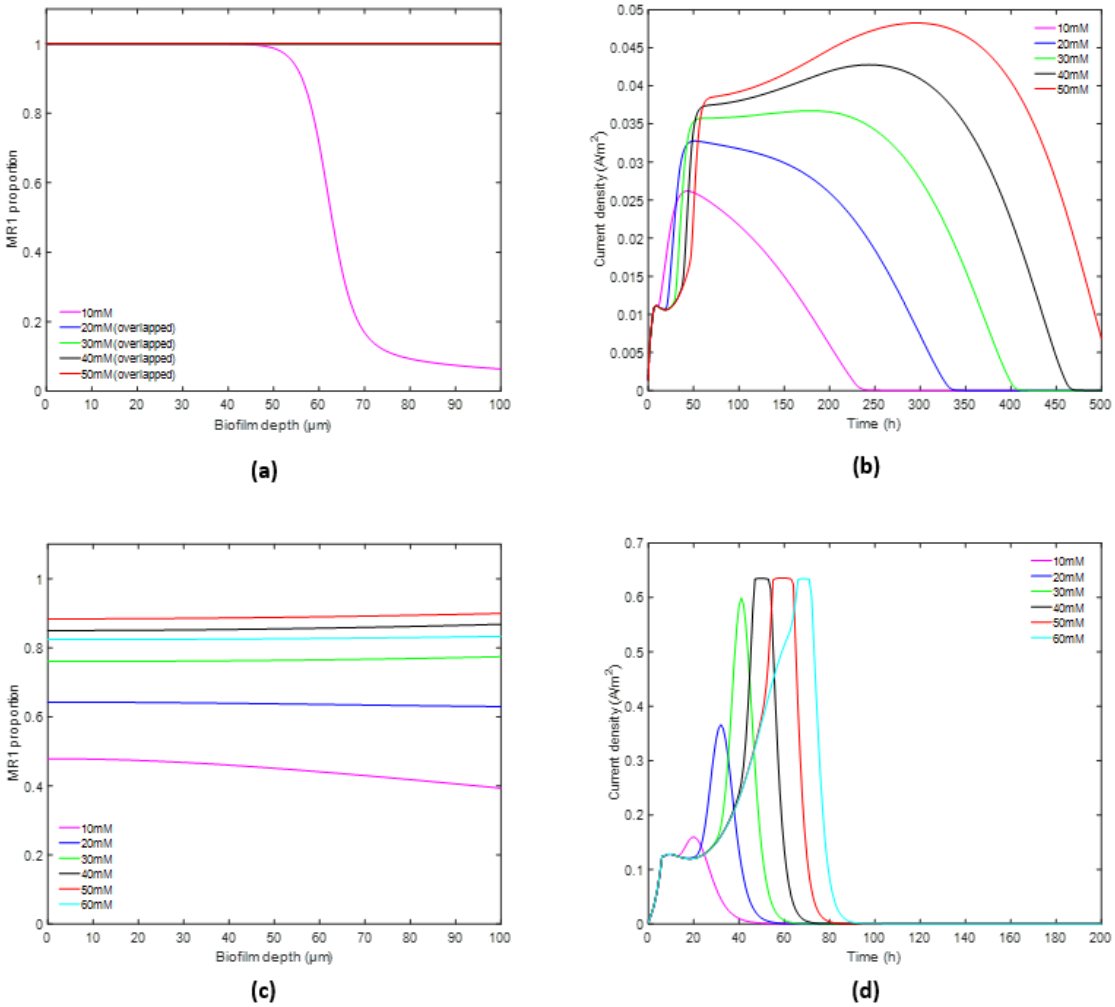

Figure 1 Model outputs of the batch MFC at different values of initial glucose concentration, $C_{P,B,0}$. (a) and (c): Batch-end MR1 proportion in the biofilm with MET and DET, respectively; (b) and (d): Current density profile with MET and DET, respectively;

In the case of MET, the co-existence of the two species can be maintained at the end of batch, only when the initial glucose concentration is the lowest among the tested levels (i.e. 10mM, as shown in Figure 1(a)), while all the higher initial glucose concentrations lead to an 'MR1-only' biofilm. The lower initial glucose supply means lower formate availability, which restricts the growth of MR1. In this case, formate is also depleted sooner and therefore MR1 stops growing within a shorter period. The combination of these two effects prevents MR1 from repelling *E. coli* completely during the batch, whereas in the cases with higher glucose supply both effects manifest in the opposite direction, leading to the exclusion of *E. coli* from the biofilm. Even in the case of sustained co-existence, the region of the biofilm closer to the anode surface is still fully occupied by MR1 thanks to its high specific growth rate in that location. The fraction of *E. coli* gradually increases towards the outer surface next to the bulk liquid phase, which is due to the combination of the decrease in the concentration of Mo (which restricts the growth of MR1) and the increase in the concentration of glucose (which promotes the growth of *E. coli*). Comparing the batch-end species distribution with the initial seeding ratio (MR1: *E. coli* = 6:4), one can see that over the batch MR1 and *E. coli* have been enriched close to the anode surface and to the bulk liquid, respectively.

It is worthy to note here that, in the cases of higher glucose supply, *E. coli* accomplishes complete glucose conversion before being repelled from the biofilm, consequently higher overall current generation is predicted with higher initial glucose concentrations (as shown in Figure 1(b)) which essentially imply greater availability of formate. However, in the early stage of the batch, a run with a higher glucose concentration is shown to produce a lower current density over a certain period of time. This is due to the less restricted initial growth of *E. coli* in that period, which leads to a lower fraction of the current-generating MR1. After that period, the increase in the availability of formate starts to become a dominating driver in the system, gradually turning MR1 to the dominant species, and hence greater current generation.

The results with DET (Figure 1(c)) show rather noticeable differences with those with MET. In terms of biofilm composition, the co-existence of the two species is maintained in all the tested cases. This is an outcome of a number of inter-connected factors. Firstly, there is less limitation to the growth of MR1 by potential (see Eq. (16)) in DET than that by M_o (see Eq. (15)) in MET. Besides, the predicted variation of potential across the biofilm is insignificant at

the assumed biofilm thickness and electrical resistance, which is in sharp contrast with the rather uneven distribution of M_o in MET as its recovery (from its reduced form) occurs only at the anode surface. The above two factors mean that compared to the MET case, the predicted growth of MR1 over the entire biofilm is significantly greater during most part of a batch (see SI, Section IV, Figure S1), and is spread relatively evenly across the biofilm resulting in a rather sizable MR1 fraction even at its outer surface. The consequence is that a significant amount of MR1 biomass is produced (before formate is depleted), a noticeable proportion of which however leaves the biofilm through detachment at the outer surface (after the biofilm reaches its assumed maximum thickness). Besides, the faster exhaustion of formate (compared to the MET cases) also means that in all the tested DET cases, MR1 is not able to completely occupy the inner part of the biofilm before the depletion of formate (see see SI, Section IV, Figure S2), and the biomass composition cross the biofilm varies rather insignificantly (see Figure 1(c)), which are both in contrast with the results of the MET model. When the initial glucose concentration increases from 10mM to 50mM, the fraction of MR1 increases, as the benefit of a greater concentration of formate (converted from glucose, favouring the growth of MR1) outweighs that of a greater glucose concentration, favouring the growth *E. coli*. The relativity of benefits eventually changes when the initial glucose concentration increases further to 60mM, leading to a reduced MR1 fraction in the biofilm.

On the predicted current density (Figure 1(d)), the impacts of glucose concentration on current density in DET are qualitatively similar to MET. However, the maximum current density achieved with DET is significantly higher than with MET, and the batch duration (marked by the time at which the current density becomes zero) of the former is much shorter than the latter. These are results of the DET case having greater averaged *specific growth rate* of MR1 (see SI, Section IV, Figure S1) and greater consumption of formate by the stronger growth of MR1 (see SI, Section IV, Figure S2).

4.1.2. *The effect of seeding ratio (MR1:E. coli)*

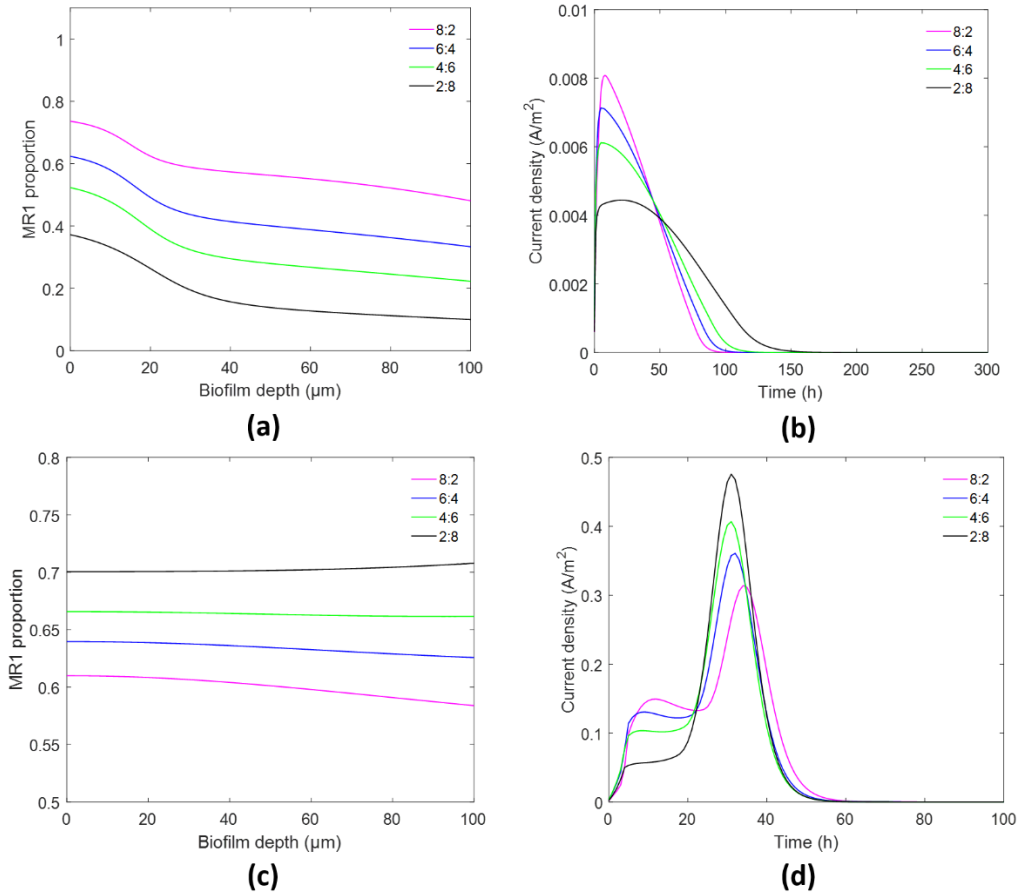

Figure 2 Model outputs of the batch MFC at different values of seeding ratios. (a) and (c): Batch-end MR1 proportion with MET when $C_{p,B,0} = 1mM$ and when with DET $C_{p,B,0} = 20mM$, respectively; (b) and (d): Current density profile with MET when $C_{P,B,0} = 1mM$ and with DET when $C_{p,B,0} = 20mM$.

Setting the initial glucose concentration to 20mM, the variation in seeding ratio did not change the dominance of the high glucose (and hence formate) availability in the predicted dynamics of the system, as confirming the similar observation described in Section 4.1.1. However, at 10mM, a level shown earlier (magenta line in Figure 1(a)) to lead to co-existence (at the default seeding ratio, 6:4), the tested seeding ratios result in qualitatively similar batch-end species distribution profiles. If we continue to decrease the initial glucose concentration $C_{P,B,0}$ to 1mM, the MR1 proportion at the anode surface changes significantly with seeding ratio, as shown in Figure 2(a). In this case, higher seeding ratios still lead to higher batch-end MR1 proportions in the biofilm, however in the case of the highest seeding ratio (8:2), MR1 proportion at the anode surface reduces from 80% to ~75% during the batch

(while an increase in predicted for the other ratios). This reduction is the victim of rapid consumption of formate by the large initial fraction of MR1 in the biofilm which causes a low formate concentration and reduces the specific growth rate of MR1. In terms of current generation, higher seeding ratios generally lead to higher peaks of current density and shorter batches, when the seeding ratio can actually affect the biofilm composition, i.e. when the system starts with a sufficiently low glucose concentration, as illustrated in Figure 2(b) for the case of $C_{P,B,0}$ = 1mM.

In the case of DET, it turns out that the order of batch-end biofilm compositions between different batches completely reverses the order of the initial seeding ratios (Figure 2(c); see Figure S3 in SI, Section V for further details). When explaining the 1mM $C_{P,B,0}$ case with MET (Figure 2(a)), we pointed out the negative effect on the specific growth rate of MR1 at the low formate concentration caused by the "over" consumption of a high initial fraction of MR1. In the cases tested with DET, this negative effect becomes much more pronounced, and leads to the observed reversion. Essentially, this means that a batch with a higher seeding ratio experiences a higher amount of MR1 in the biofilm (compared to a batch with a lower seeding ratio) in the early stage of the batch, and then moves to a biofilm composition with a lower amount of MR1. This is also reflected by the trends of current generation, as shown in Figure 2(d): a batch with a higher (lower) seeding ratio has a higher (lower) level of current density initially, and then transits to a lower (higher) level.

4.1.3. *The effect of maximum biofilm thickness,* $L_{F,max}$

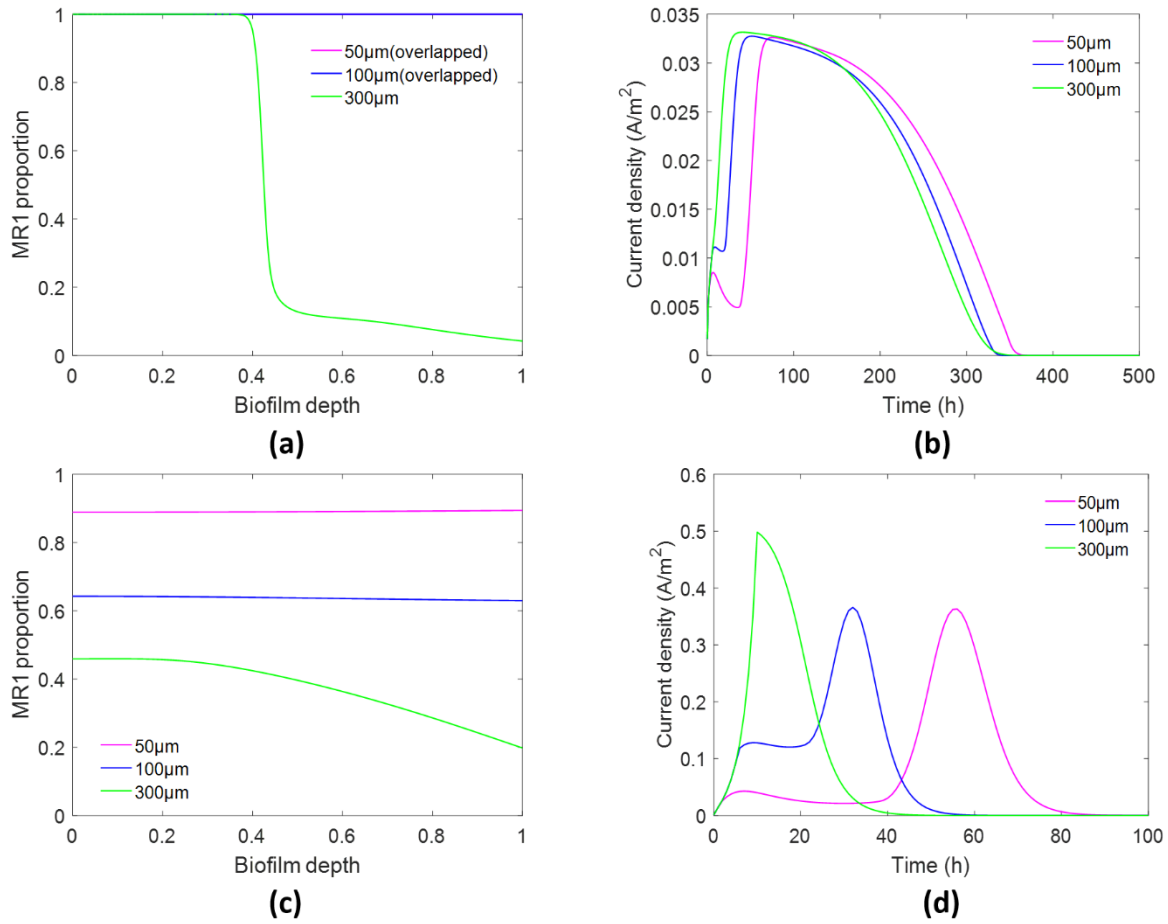

Figure 3 Model outputs of the batch MFC at different values of maximum biofilm thickness, $L_{F,max}$. (a) and (c): Batch-end MR1 proportion in the biofilm with MET and DET, respectively; (b) and (d): Current density profile with MET and DET, respectively.

With MET, the increase in biofilm thickness causes the biofilm type to shift from 'MR1-only' to 'MR1-*E. coli* co-existing' (see Figure 3(a)). The biofilm composition is closely related to Mo and formate concentration profiles within the biofilm. As the biofilm is set to greater thickness, the concentrations of formate and Mo are more hindered by diffusion resistance. Subsequently, the specific growth rate of MR1 is limited and MR1 cannot occupy the entire biofilm. On current generation, one can see from Figure 3(b) that the change in biofilm thickness causes little difference in the maximum current density. However, the two batches with lower thickness experience an apparent dip in current density after the biofilm grows to its maximum thickness. This is caused by the longer period of repulsion by *E. coli* to MR1 in these thinner biofilms which itself is due to longer availability of glucose.

In the case of DET, co-existence of the two species is predicted with all the three thickness levels; the overall proportion of MR1 is lower in a thicker biofilm (Figure 3(c)). Analogous to the effect of a thicker biofilm on formate and Mo concentrations with MET, formate concentration and electrical potential are lower with a thicker biofilm in the case of DET, leading to slower growth of MR1. The more obvious change of MR1 proportion with location in the thickest biofilm is attributed to the increasing variation of electrical potential and formate concentration across the biofilm. The trend of current density with DET is similar as MET, but with stronger initial decrease in the two thinner biofilm. This is because of the faster formate consumption (hence weaker competitiveness of MR1) with DET, compared to the corresponding batch with MET, during the "dipping" period (Figure 3(d)).

4.1.4. The effect of external resistance, R_{ext}

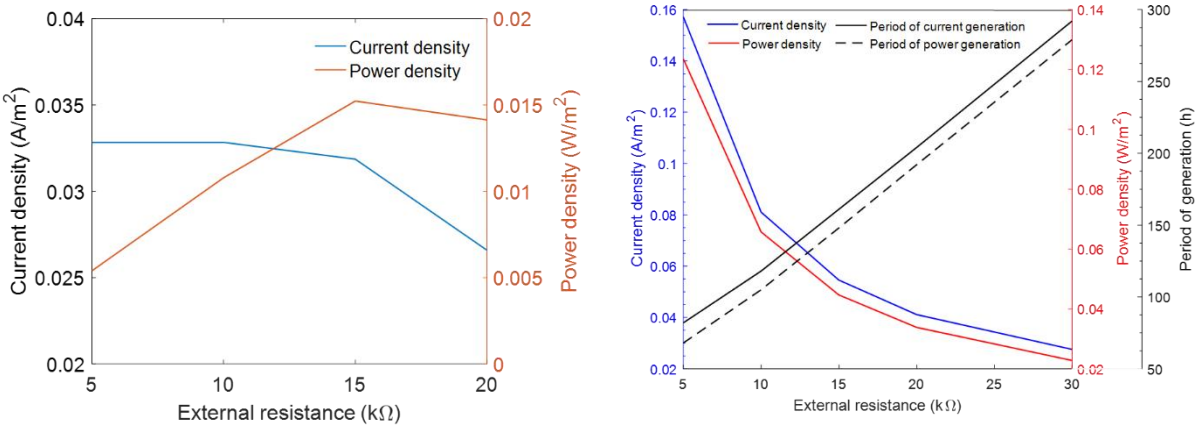

Figure 4 Model outputs of the batch MFC at different values of external resistance, R_{ext}.(a) with MET; (b) with DET.

The effect of R_{ext} on biofilm composition in the batches modelled with MET turns out to be insignificant, as a 'MR1-only' biofilm is always obtained at the end (results not shown). Besides, the simulation results suggest that the current density is insensitive to R_{ext} when R_{ext} is smaller (<10kΩ) (see Figure 4(a)). There are two factors that determine current generation in the case of MET: anode potential and M_r concentration at the anode surface. The anode potential is higher when R_{ext} is smaller, which has a direct positive impact on the rate of M_r oxidation ($M_r \rightarrow M_o$) at the anode surface. However, this also makes M_r harder to

accumulate (see SI, Section VI, Figure S4), which limits the oxidation process. The combined effect of the above two factors is that the difference in current density between different R_{ext} is rather insignificant at the lower range of R_{ext}. However, when R_{ext} becomes larger (>10kΩ), the influence of a lower anode potential is more significant and dictates the slower rate of the M_r oxidation process. Therefore, the peak current density decreases noticeably. In terms of power density, as the product of current density and R_{ext}, it shows a peak at R_{ext} = 15 kΩ (Figure 4(a)).

With DET, higher R_{ext} is beneficial for MR1 to occupy the biofilm by the end of a batch, with MR1 occupying the entire biofilm when R_{ext} exceeds 30kΩ (see SI, Section VI, Figure S5). We find that electrical potential in the biofilm drops significantly with a higher R_{ext}, which limits the specific growth rate of MR1. On the other hand, the restricted growth of MR1 also means lower consumption and therefore more sustained availability of formate, which enables MR1 to continue its growth for a longer period (corresponding to the period of current generation, see SI, Section VI, Figure S6). Consequently, the fraction of MR1 is able to eventually recover and even dominates the biofilm. In terms of current generation, the batches with higher electrical resistance are predicted to have a lower peak current (and power) density but a longer period of active current (and power) generation, as shown in Figure 4(b).

4.1.5. The effect of initial concentration of the oxidized form of the mediator in the bulk liquid, $C_{Mo,B,0}$

In the case of MET, the batch-end biofilm composition changes from 'MR1-only' to 'MR1-*E. coli* co-existing' type with M_o increase (see SI, Section VII, Figure S7(a)). In Section 4.1.2, we have pointed out that a higher MR1:*E. coli* seeding ratio can lead to faster formate consumption which hinders the occupation of the biofilm by MR1. A similar effect is caused here by a higher M_o. With respect to current generation, faster formate consumption caused by a higher initial concentration of *Mo* leads to an earlier and higher peak current density, and a shorter duration of current production, as shown in Figure S7(b) (see SI, Section VII).

4.2. Continuous mode

With the continuous mode, our interest lies in the longer-term behaviour and performance of the MFC, which appeared from the conducted simulation runs to be insensitive to the initial glucose concentration $C_{P,B,0}$ in the bulk liquid and the seeding ratio, therefore the results of the simulations aimed to show their influence are not reported here. Besides, the effect of external resistance on the biofilm composition was shown to be negligible. The predicted power generation showed the same characteristics in simulations with the two different EET mechanisms: the current density decreases with the increasing external resistance, and an optimal value of external resistance exists and corresponds to a maximum power density, both of which are in accordance with the previously reported experimental finding [42]. As no insights manifested additionally to those already revealed by the batch mode with respect to the impact of external resistance, the simulation results pertaining to this parameter are not further discussed. The rest of this section will thus focus on the impact of two important parameters for a continuous bioreactor, namely flowrate (which determines dilution) and inlet substrate (i.e. glucose in this case) concentration, as well as biofilm thickness which shows multiple effects in the earlier analysis of the batch mode. Besides, one initial condition, namely the initial *Mo* concentration in the bulk liquid, was shown to affect the long-term composition of the biofilm, hence the relevant results are presented here. Unless stated otherwise, the results shown are of a steady state reached by the continuous reactor.

4.2.1. *The effect of flowrate, V_f*

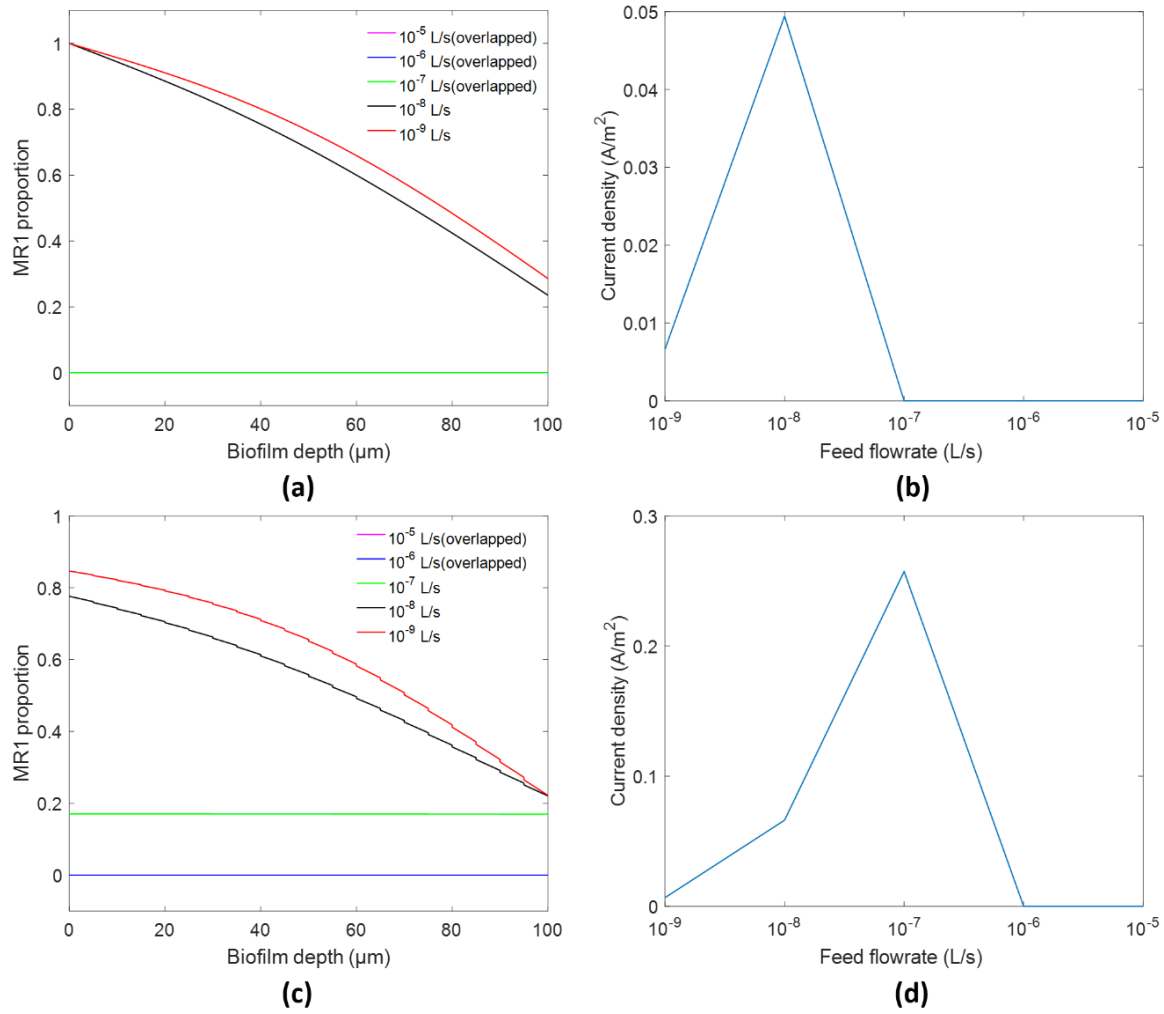

Figure 5 Model outputs of the continuous MFC at different values of flowrate, V_f. (a) and (c): MR1 proportion in the biofilm at the steady state with MET and DET, respectively; (b) and (d): Current density profile with MET and DET, respectively.

The results for the MET model are shown in Figure 5(a) and (b). With the feeding flowrate being $1 \times 10^{-7} L/s$ or higher, MR1 is shown to be completely repelled from the biofilm, which is due to the significant dilution impact leading to a low formate concentration that causes severe restrictions to the growth of MR1. This means collapse of the 'fermenter-EAB' consortium, and hence the failure of the system to produce current. When the flowrate is reduced to $1 \times 10^{-8} L/s$, the anode chamber becomes able to accumulate formate to a level that allows MR1 to compete with *E. coli* for the space in the biofilm, leading to a biofilm composition profile similar to those observed earlier in the batch reactor (with MET). As the

two-species consortium is stably present, continuous current generation is sustained. Further reduction of the flowrate improves the competitiveness of MR1 in the biofilm, however the lower supply of glucose leads to the reduction of current density.

For DET, Figure 5(c) and (d) show that in general, biofilm composition and current generation follow a tendency of changes with flowrate similar to the case of MET. It is noticeable, however, the biofilm transfer from '*E. coli*-only' to '*E. coli*-MR1 co-existing' via a special occasion with unvaried distribution of the two species cross the biofilm, at a flowrate of $1 \times 10^{-7} L/s$. In this occasion, the formate concentration is high enough to increase the specific growth rate of MR1 (compared to the cases with higher flowrates) to the same level of *E. coli* before *E.coli* completely occupies the biofilm. At steady state, this identical specific growth rate of MR1 and *E.coli* dictates a zero spatial gradient of the biomass fractions in the biofilm (see SI, Section VIII for a proof).

4.2.2. The effect of inlet concentration of primary substrate (glucose), $C_{P,in}$

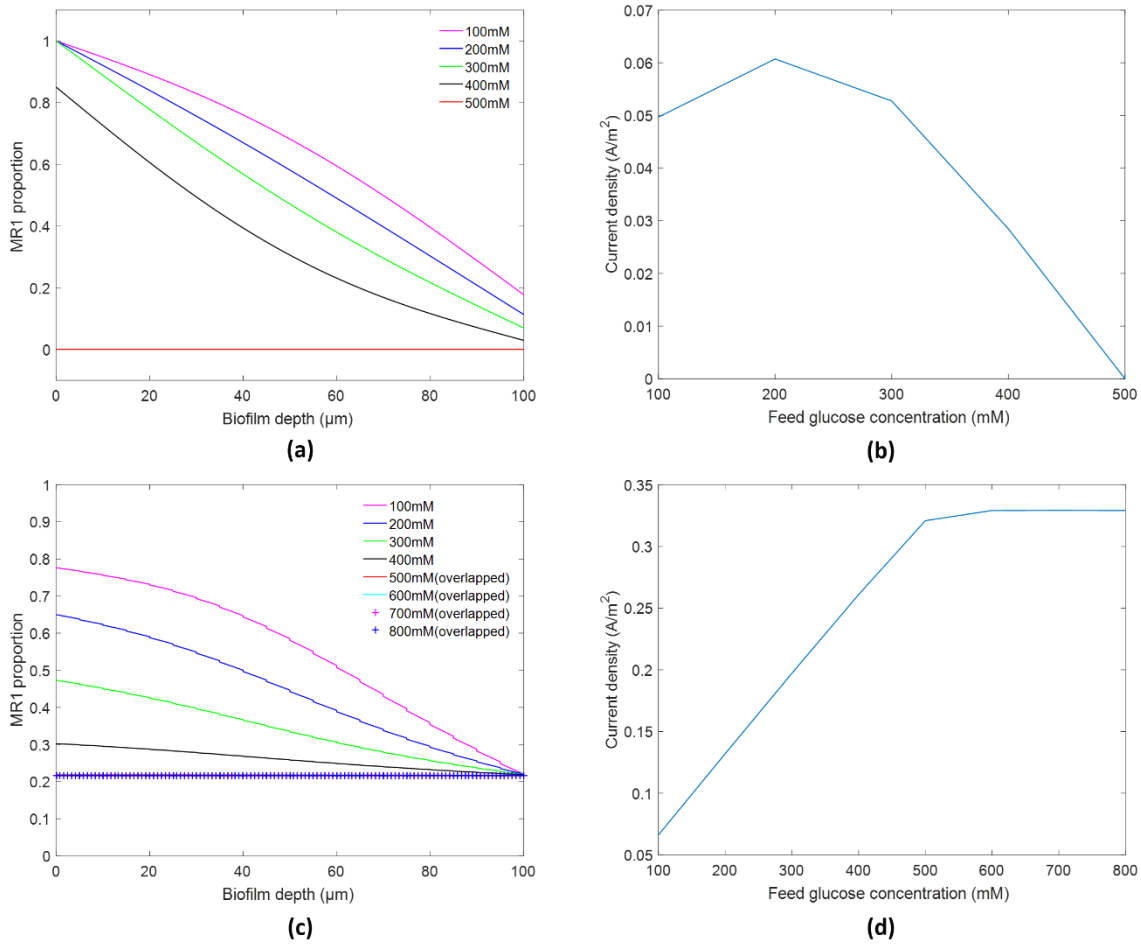

Figure 6 Model outputs of the continuous MFC at different values of inlet glucose concentration, $C_{P,in}$. (a) and (c): MR1 proportion in the biofilm at the steady state with MET and DET, respectively. (b) and (d): Current density profile with MET and DET, respectively.

As shown in the Figure 6(a), a continuous MFC governed by MET is predicted to have *E. coli* repelling MR1 from the biofilm strongly when the system is fed with more concentrated glucose, with *E. coli* occupying the biofilm completely when $C_{P,in}$ increases to 500mM. At the biofilm inner surface, the specific growth rate of *E. coli* rises significantly when $C_{P,in}$ is increased to 400mM as it to a large extent reduces the glucose limitation to the growth of *E. coli* even at this most remote location for glucose supply. Although the increased *E. coli* growth also means better supply of formate, the specific growth rate of MR1 starts to decline at a certain point due to the limitation by M_o following the fast initial consumption resulting from the abundant substrate supply. These two causes collectively lead to the predicted decline and eventual exclusion of MR1 from the biofilm as $C_{P,in}$ increases. On current generation, Figure 6(b) shows that the current density boosts firstly as the greater supply of the substrate plays a more dominant role. After that, it decreases, dictated by the decline of the fraction of MR1 in the biofilm.

In the case of DET, the fraction of MR1 in the biofilm also shows a declining trend as $C_{P,in}$ increases. However, unlike the case of MET where MR1 is eventually repelled completely, here an upper limit (~80%) is predicted for the proportion of *E. coli* (Figure 6(c)). This is because, compared to the significant influence of the reduction in M_o concentration in the case of MET, the level of the anode potential in the case of DET allows the specific growth rate of MR1 to eventually stabilise at a level equal to that of *E. coli*, resulting in the co-existing, even distribution of the two species across the biofilm. On current generation, the case of DET is shown (Figure 6(d)) to be dominated by the supply of the substrate (via the *specific growth rate* of MR1, as opposed to the *fraction* of MR1 in the biofilm) with increase in current density until the substrate supply reaches a saturated level.

4.2.3. *The effect of maximum biofilm thickness, $L_{F,max}$*

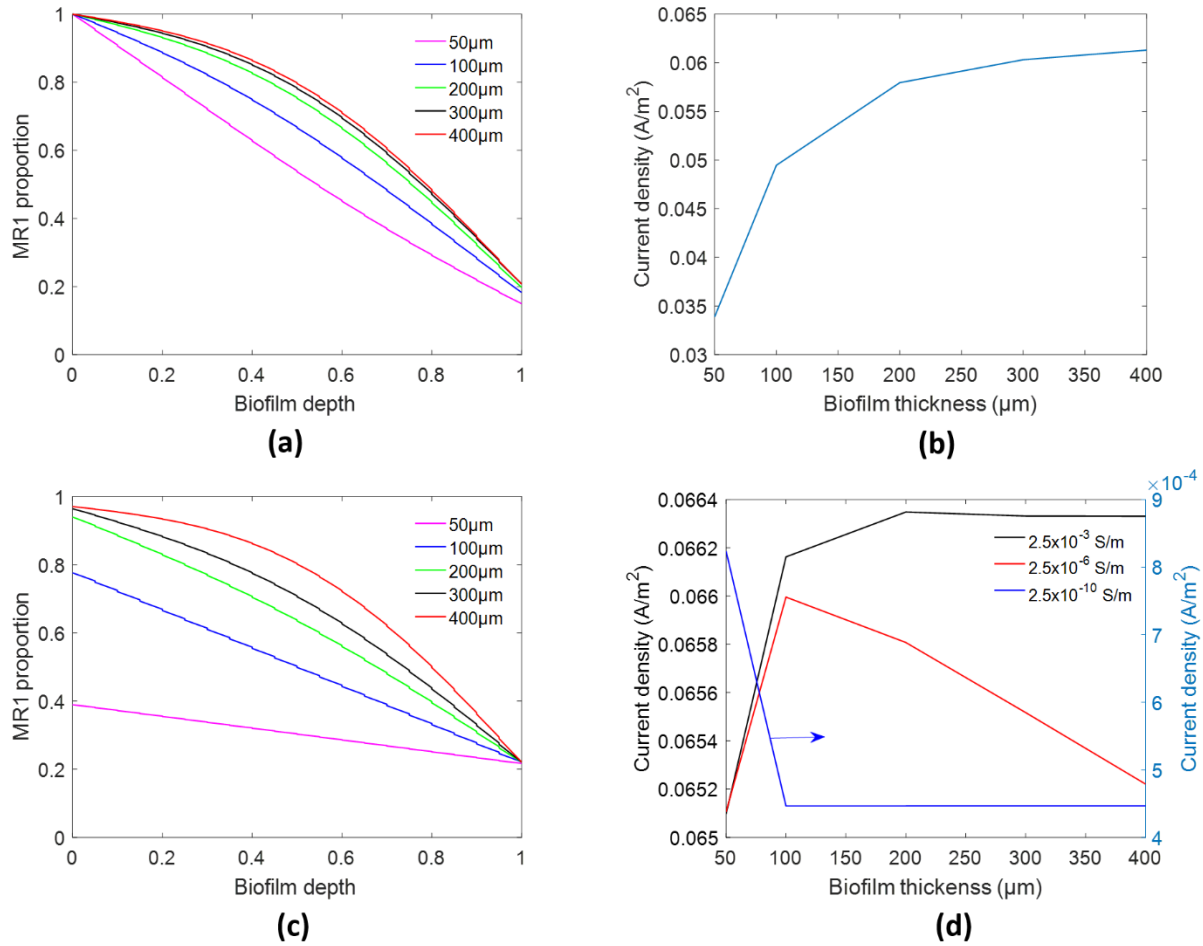

Figure 7 Model outputs of the continuous MFC at different values of the maximum biofilm thickness, L_{fmax}. (a) and (c): MR1 proportion in the biofilm at the steady state with MET and DET, respectively; (b) and (d): Current density with MET and DET, respectively.

In the case of MET, it can be seen from Figure 7(a) that the proportion of MR1 in the biofilm increases with the thickness of the biofilm, which is due to the negative effect of a thicker biofilm on the growth of *E. coli* via the impediment of the diffusion of glucose from the bulk liquid. The gain in the fraction of MR1 in a thicker biofilm however decreases as the thickness increases, because of the negative impact of the impeded diffusion of glucose on the supply of formate. Accordingly, the current density shows an increasing trend with the biofilm thickness, but at a reduced increment, as presented in Figure 7(b).

Compared to MET, the DET case is affected by the biofilm thickness via another factor additional to the impediment on glucose diffusion: electrical resistance (and hence potential) within the biofilm matrix. However, the results shown in Figure 7(c), similar to that of MET, are primarily dictated by glucose diffusion, since at the default electrical conductivity of the biofilm ($2.5 \times 10^{-3}\ S/m$) the potential gradient within the biofilm is negligible. With hypothetical lower conductivity values, the impact of potential becomes more predominant, as can be seen in Figure 7(d). The figure shows that, with a higher conductivity ($2.5 \times 10^{-3}\ S/m$), the current density increases with biofilm thickness when the biofilm is thinner than 200μm, due to the dominating effect of the increased fraction of MR1 in the biofilm. Beyond this thickness, the current density has no obvious further improvement, because of the combined effect of the two factors that generally affect the current density, namely the increase in MR1 fraction and the decrease in the specific growth rate of MR1 (mainly due to the reduction in formate availability at this particular level of conductivity). With lower conductivities, overall the biofilm generates smaller current densities, which is not surprising as higher electrical resistance causes lower electrical potential and hence slower growth of MR1.

Figure 7(d) also shows that when the biofilm conductivity is $2.5 \times 10^{-6}\ S/m$, there is an optimal biofilm thickness within the tested range, which corresponds to a maximum current density, suggesting that the disadvantage of a thicker biofilm (causing potential drop across the biofilm) becomes increasingly pronounced and eventually overweighs the advantage of the increase in MR1 fraction. When the biofilm conductivity is the lowest, i.e. $2.5 \times 10^{-10}\ S/m$, the lower MR1 specific growth rate (now significantly caused by the reduction of potential across the biofilm) is the major determinant of current generation: the current density decreases first as the biofilm thickness increases and then sustains a constant level by the compensation of a higher MR1 biomass fraction in the thicker biofilm.

4.2.4. The effect of initial concentration of the oxidized form of the mediator in the bulk liquid, $C_{Mo,B,0}$

It turns out that the impact of initial *Mo* concentration, $C_{Mo,B,0}$ on the steady-state biofilm composition, in MET-based systems, is dependent of inlet concentration of primary substrate (glucose),$C_{p,in}$, as shown in Table 1.

587 *Table 1 Variation of biofilm composition with $C_{Mo,B,0}$ and $C_{P,in}$*

$C_{Mo,B,0}$	$C_{P,in}$=100mM	$C_{P,\mathrm{in}}$=300mM	$C_{P,\mathrm{in}}$=500mM
0mM 1×10^{-5}mM 1×10^{-3}mM 1×10^{-1}mM	*E. coli*-MR1 co-existence	*E. coli* only *E. coli*-MR1 co-existence	*E. coli* only

588 The steady-state biofilm composition does not change with the initial *Mo* concentration when
589 $C_{P,\mathrm{in}}$ is as either 100mM or 500mM. At the lower $C_{P,\mathrm{in}}$, the *Mo* concentration in the biofilm is
590 able to sustain the specific growth rate of MR1 and is not consumed rapidly, hence allowing
591 for the two species to co-exist. At the higher $C_{P,\mathrm{in}}$, none of the tested *Mo* values can sustain
592 the consumption by the growth of MR1 and will become depleted eventually. Together with
593 the fact that a higher $C_{P,\mathrm{in}}$ is also beneficial for *E. coli* growth, an '*E. coli*-only' biofilm results
594 with all the tested initial *Mo* concentrations, and this result is consistent with the earlier
595 discussion on the impact of $C_{P,\mathrm{in}}$ (see Section 4.2.2). When $C_{P,\mathrm{in}}$ equals to 300mM, however,
596 the increase in the initial *Mo* concentration appears to be able to cause changes to the stable
597 biofilm composition, with the biofilm shifts from '*E. coli*-MR1 co-existing' to '*E. coli*-only'.
598 Among the tested levels of the initial *Mo* concentration, the "middle" value of 1×10^{-3}mM
599 appears to mark the transition in the ability of the available *Mo* to sustain MR1 in the biofilm.

600 **5. Discussion**

601 5.1. Batch vs. continuous reactors

602 The nature of a batch reactor means that the evolution of its dynamics terminates once all
603 the substrates are completely consumed, whereas a continuous reactor has the chance to
604 unfold its dynamics without such a time limitation. Due to this difference, the initial conditions
605 significantly affect the biofilm composition and current generation in the batch mode, which
606 however often do not have an impact on the long-term state of the continuous reactor (with
607 the exception of the initial M_o concentration in the case of MET). Taking seeding ratio as an
608 example, our simulation results show that the initial setting clearly influence the end state of
609 the batch reactor through distinct mechanisms and dynamics with MET and DET. In a
610 continuous reactor, such dynamics could also be experienced in the early stage of the
611 operation, yet the further evolution of the dynamics would eventually eliminate the influence
612 of the difference in the initial setting. On the impact of other parameters settings, the

theoretically infinitely long period of operation, together with the continued supply of substrate, could lead to rather different outcomes in the continuous reactor than its batch counter-part. In fact, it was the case of the maximum biofilm thickness: MR1 proportion decreases with biofilm thickness in the batch mode, while an opposite trend manifests in the continuous mode with both EET mechanisms.

In both batch and continuous reactors, optimal parameter settings could be identified from the simulation results, although in different senses. With a continuous reactor, steady-state power output can be used as a clear objective, which can only be delivered by parameter settings that result in a stable consortium. From Table S3(b)(see SI, Section IX), one can see such parameter settings, which are typically those that lead to the "best" composition of the biofilm, i.e. those resulting in the ideal combination of the amount of MR1 in the biofilm and its overall specific growth rate. For a batch reactor, all the tested cases showed complete conversion of the original substrate (glucose) regardless of the final composition of the biofilm. However, in terms of power generation, batches with certain parameter settings are predicted to have a higher peak current density and a shorter period needed for complete conversion (see SI, Section IX, Table S3(a)), which may be considered as more desirable than the others parameter settings.

5.2. MET vs. DET

From the model description, one can see that with both EET mechanisms, current generation is primarily determined by the growth of MR1, either directly as with DET or indirectly as with MET (which is through affecting the generation of the reduced mediator). In the case of MET, the specific growth rate of MR1 is affected by the concentration of M_o, which is replaced by the potential in the biofilm in the case of DET. In the Results section, we have already stated one important implication of this difference: As M_o is regenerated by oxidation only at the anode surface, its concentration declines rapidly in the biofilm towards the outer surface. In contrast, the electrical potential tends to have minor variation across the biofilm except when its electrical resistance is extremely high. This difference underlies several general observations relating to the comparison of DET with MET, including a lesser degree of spatial variation in the fractions of the two species, greater overall growth of MR1 in the biofilm, and higher attainable current density. There is yet another aspect of the difference between the

role of M_o in MET and that of potential in DET: A positive feedback loop exists with M_o and the growth of MR1, in that a higher M_o concentration can escalate the proportion of MR1 in the biofilm; the increased amount of MR1 in turn produces more M_o. In contrast, a higher potential can improve the growth of MR1 and hence current generation, which however would lead to the increase of the potential loss by the external load, i.e. to a reduction to the potential at the anode surface and hence across the biofilm, hence forming a negative feedback loop. None of these two loops would function in isolation with other aspects of the dynamics of the reactor, yet the difference between them means that temporal variation of M_o could bring influence more significantly to an MET system than that of the potential to a DET system.

In this work, these two EET mechanisms have been studied separately. There is experimental evidence that shows the co-functioning of MET and DET in certain systems [43]. It would be interesting for the future work to model a multi-species anodic biofilm with dual EET mechanisms, building on an existing model [12].

5.3. Trade-offs and their implications

It is noticeable that biofilm composition response and current generation performance are often the result of various trade-offs between multiple impacts of individual factors. For example, the initial glucose concentration in a batch reactor and the feed glucose concentration in a continuous reactor affect both the growth rate of *E. coli* (directly) and that of MR1 (via formate concentration). In a continuous reactor, its flowrate affects both substrate supply and dilution. In both types of reactors, biofilm thickness impacts on the amount of biomass the biofilm can accommodate and on the resistances to mass transfer and current conduction. In each pair of such trade-off impacts, their relevant dominance determines the "net" impact of the impacting factor, which however may shift with the variation in the magnitude of some other parameter settings, as observed, for example, in the predicted variation of the steady-state current density against biofilm thickness in the continuous reactor with DET and an intermediate level of biofilm conductivity (see Section 4.2.3). The trade-offs and their shifts have shown in several cases to lead to the existence of an optimal parameter value, such as 15kΩ for the external resistance in batch with MET; 1×10^{-8} and $1 \times 10^{-7} L/s$ for the flowrate in the continuous MFCs with MET and DET,

673 respectively; and 100μm for the biofilm thickness with moderate conductivity (i.e. $2.5 \times$
674 $10^{-6}\ S/m$) in the continuous MFC with DET. It should be mentioned that biofilm composition
675 and current generation may show different trends from the impact of the various factors and
676 trade-offs, as the former is primarily affected by the comparative specific growth rate of the
677 two microbes at different locations of the biofilm, while the latter is largely affected by the
678 overall amount of MR1 biomass in the biofilm and its overall (or average) specific growth rate.

679 **6. Conclusions**

680 Detailed simulation studies were carried in this work on MFCs with an anodic biofilm
681 populated with a 'fermenter-EAB' two-species microbial consortium. The results reveal the
682 responses of biofilm composition and current generation to a range of chemical, biological
683 and physical factors via two different EET mechanisms (MET and DET) and under two
684 operating modes (batch and continuous). The outcome of a batch MFC was shown to be
685 significantly influenced by all the initial conditions, while the oxidised mediator concentration
686 appeared to be the only initial condition that affects the steady state of a continuous MFC
687 (with MET). The two operating modes also showed contrasting responses to the maximum
688 biofilm thickness, while the continuous mode additionally showed critical impacts of flowrate
689 and the inlet substrate concentration on the stability of the consortium and on the relative
690 species abundance across the biofilm. Between MET and DET, the different roles and spatial
691 distribution profiles of oxidised mediator concentration (relevant to MET) and electrical
692 potential (relevant to DET) were shown to dictate a number of key differences in the predicted
693 outcomes of the two EET mechanisms. Generally, biofilm composition and current generation
694 in the simulated MFCs are shaped by the trade-offs that exist between multiple impacts of
695 individual factors in all the simulated cases, reflecting the interplay between microbial growth,
696 mass transfer, and electrical conduction. Our simulation results also suggested that optimal
697 settings exist with several parameters leading to reduced batch duration or enhanced
698 continuous power generation.

699 **Conflicts of interest**

700 There are no conflicts to declare.

701 **Nomenclature**

E^0	Standard mediator redox potential, V
E_{KA}	Potential corresponding half-maximum specific growth rate, V
R_{ext}	External resistance, Ω
R_{ideal}	Ideal gas constant, $J/(mol \cdot K)$
R_{int}	Internal resistance, Ω
V_a	Anode potential, V
V_c	Cathode potential, V
i_o	Exchange current density, A
k_a	Oxidation rate constant, m/s
k_c	Reduction rate constant, m/s
A	Area, m^2
C	Concentration, mol/m^3
D	Diffusion coefficient, m^2/s
F	Faraday constant, C/mol
J	Exchange mass flow, $mol/(m^2 \cdot s)$
K	Half-saturation constant, mol/m^3
L	Thickness, m
R	Reaction rate, $mol/(m^3 \cdot s)$ or $kg/(m^3 \cdot s)$
T	Operating temperature, K
V	Volume, m^3
X	Biomass concentration, kg/m^3
Y	Yield coefficient, dimensionless

f	Fraction of electrons recoverable from EAB's substrate for current, dimensionless
i	Current density, A/m^2
k	Biofilm conductivity, S/m
n	Electron transferred per redox mediator reaction, dimensionless
r	Reaction rate at the anode surface, $mol/(m^2 \cdot s)$
t	Time, s
v	Advective velocity, m/s
x	The direction along biofilm depth
y	Electron equivalence of EAB's substrate for current generation, dimensionless
β	Transfer coefficient for mediator oxidation/reduction reaction, dimensionless
ε	Porosity, dimensionless
ζ	Converted coordination, same as x direction
μ	Biomass specific growth rate, $1/s$
ρ	Density, kg/m^3

Subscripts

0	Initial state, t=0
B	Bulk liquid
C	DET
D	Diffusion layer
E	Electrode

EA	Electron acceptor
FB	Fermentative bacteria
EAB	Electrochemically Active Bacteria
F	Biofilm
I	Intermediate substrate (EAB's substrate)
M	MET
Mo	Oxidised form of the mediator (FMN)
Mr	Reduced form of the mediator ($FMNH_2$)
P	Primary substrate
S	Dissolved soluble component
X	Biomass
f	Flow
in	Inlet flow
max	Maximum
ox	Oxidation process
red	Reduction process
ref	Reference condition

Abbreviation

BESs	Bioelectrochemical systems
DET	Direct conduction-based extracellular electron transfer
E. coli	*Escherichia coli*
EA	Electron acceptor
EAB	Electrochemically active bacteria

EET	Extracellular electron transfer
FB	Fermentative bacteria
MET	Mediator-based extracellular electron transfer
MFCs	Microbial fuel cells
S. oneidensis	*Shewanella oneidensis*

Acknowledgement

This work was supported by China Scholarship Council (CSC).

References

[1] R.M. Allen, H.P. Bennetto, Microbial Fuel-Cells: Electricity production from carbohydrates, Appl. Biochem. Biotechnol. 39 (1993) 27–40.

[2] F. Harnisch, U. Schröder, From MFC to MXC: chemical and biological cathodes and their potential for microbial bioelectrochemical systems, Chem. Soc. Rev. 39 (2010) 4433–4448. https://doi.org/10.1039/c003068f.

[3] Y.Y. Yu, D.D. Zhai, R.W. Si, J.Z. Sun, X. Liu, Y.C. Yong, Three-dimensional electrodes for high-performance bioelectrochemical systems, Int. J. Mol. Sci. 18 (2017). https://doi.org/10.3390/ijms18010090.

[4] S. Cheng, B.E. Logan, Sustainable and efficient biohydrogen production via elecctrohydrogenesis, Proc. Natl. Acad. Sci. U.S.A. 104(2007) 18871-18873. https://doi.org/10.1073/pnas.0706379104.

[5] R.A. Rozendal, A.W. Jeremiasse, H.V.M. Hamelers, C.J.N. Buisman, Hydrogen production with a microbial biocathode, Environ. Sci. Technol. 42 (2008) 629–634. https://doi.org/10.1021/es071720+.

[6] R.A. Rozendal, E. Leone, J. Keller, K. Rabaey, Efficient hydrogen peroxide generation from organic matter in a bioelectrochemical system, Electrochem. Commun. 11 (2009) 1752–1755. https://doi.org/10.1016/j.elecom.2009.07.008.

[7] M. Villano, F. Aulenta, C. Ciucci, T. Ferri, A. Giuliano, M. Majone, Bioelectrochemical reduction of CO2 to CH4 via direct and indirect extracellular electron transfer by a hydrogenophilic methanogenic culture, Bioresour. Technol. 101 (2010) 3085–3090. https://doi.org/10.1016/j.biortech.2009.12.077.

[8] S. Cheng, D. Xing, D.F. Call, B.E. Logan, Direct biological conversion of electrical current into methane by electromethanogenesis, Environ. Sci. Technol. 43 (2009) 3953–3958. https://doi.org/10.1021/es803531g.

[9] B.E. Logan, Exoelectrogenic bacteria that power microbial fuel cells, Nat. Rev. Microbiol. 7 (2009) 375–381.

[10] M.H. Do, H.H. Ngo, W.S. Guo, Y. Liu, S.W. Chang, D.D. Nguyen, L.D. Nghiem, B.J. Ni, Challenges in the application of microbial fuel cells to wastewater treatment and energy production: a mini review, Sci. Total Environ. 639 (2018) 910-920. https://doi.org/10.1016/j.scitotenv.2018.05.136.

[11] A. Okamoto, K. Hashimoto, K.H. Nealson, R. Nakamura, Rate enhancement of bacterial extracellular electron transport involves bound flavin semiquinones, Proc. Natl. Acad. Sci. 110 (2013) 7856–7861, https://doi.org/10.1073/pnas.1220823110.

[12] R. Renslow, J. Babauta, A. Kuprat, J. Schenk, C. Ivory, J. Fredrickson, H. Beyenal, Modeling biofilms with dual extracellular electron transfer mechanisms, Phys. Chem. Chem. Phys. 15 (2013) 19262–19283.

[13] B.E.R. Andrew Kato Marcus, Ce´sar I. Torres, Conduction-based modeling of the biofilm anode of a microbial fuel cell, Biotechnol. Bioeng. 98 (2007) 1171–1182.

[14] W. Habermann, E.H. Pommer, Biological fuel cells with sulphide storage capacity, Appl. Microbiol. Biotechnol. 35 (1991) 128–133, https://doi.org/10.1007/BF00180650.

[15] Y. Yang, Y. Wu, Y. Hu, Y. Cao, C.L. Poh, B. Cao, H. Song, Engineering electrodeattached microbial consortia for high-performance xylose-fed microbial fuel cell, ACS Catal. 5 (2015) 6937–6945.

[16] T. Liu, Y.Y. Yu, T. Chen, W.N. Chen, A synthetic microbial consortium of Shewanella and Bacillus for enhanced generation of bioelectricity, Biotechnol. Bioeng. 114 (2017) 526–532.

753 [17] V.B. Wang, K. Sivakumar, L. Yang, Q. Zhang, S. Kjelleberg, S.C.J. Loo, B. Cao,
754 Metabolite-enabled mutualistic interaction between Shewanella oneidensis and
755 Escherichia coli in a co-culture using an electrode as electron acceptor, Sci. Rep. 5
756 (2015) 1–11, https://doi.org/10.1038/srep11222.

757 [18] Z. Ren, T.E. Ward, J.M. Regan, Electricity production from cellulose in a microbial fuel
758 cell using a defined binary culture, Environ. Sci. Technol. 41 (2007) 4781–4786,
759 https://doi.org/10.1021/es070577h.

760 [19] A. Anna Prokhorova, B. Katrin Sturm-Richter, a Andreas Doetsch, C. Johannes
761 Geschera, Resilience, dynamics, and interactions within a model multispecies
762 exoelectrogenic-biofilm community, Appl. Environ. Microbiol. 83 (2017),
763 https://doi.org/10.1128/AEM.03033-16.

764 [20] H.S. Tong Lin, Xue Bai, Hu Yidan, Bingzhi Li, Ying-Jin Yuan, Synthetic Saccharomyces
765 cerevisiae-Shewanella oneidensis consortium enables glucose-fed high-Performance
766 microbial fuel cell, AIChE J. 63 (2017) 1830–1838, https://doi.org/10.1002/aic.15611.

767 [21] C. Picioreanu, K.P. Katuri, I.M. Head, M.C.M. Van Loosdrecht, K. Scott, Mathematical
768 model for microbial fuel cells with anodic biofilms and anaerobic digestion, Water Sci.
769 Technol. 57 (2008) 965–971, https://doi.org/10.2166/wst.2008.095.

770 [22] C. Picioreanu, M.C.M. van Loosdrecht, T.P. Curtis, K. Scott, Model based evaluation of
771 the effect of pH and electrode geometry on microbial fuel cell performance,
772 Bioelectrochemistry 78 (2010) 8–24,
773 https://doi.org/10.1016/j.bioelechem.2009.04.009.

774 [23] P. Belleville, G. Merlin, J. Ramousse, J. Deseure, Two-dimensional modelling of
775 syntrophic glucose conversion in bioanodes for coulombic efficiency optimization,
776 Bioresour. Technol. Rep. 6 (2019) 15–25,
777 https://doi.org/10.1016/j.biteb.2019.02.002.

778 [24] X.-H. Zhou, Y.-Q. Qiu, H.-C. Shi, T. Yu, M. He, Q. Cai, A new approach to quantify spatial
779 distribution of biofilm kinetic parameters by in situ determination of oxygen uptake
780 rate (OUR), Environ. Sci. Technol. 43 (2009) 757–763.

781 [25] N. John, E.T.-A. Karen, Electrochemical Systems, third, John Wiley & Sons,Hoboken,
782 New Jersey, US, 2004.

783 [26] C. Picioreanu, I.M. Head, K.P. Katuri, M.C.M. van Loosdrecht, K. Scott, A
784 computational model for biofilm-based microbial fuel cells, Water Res. 41 (2007)
785 2921–2940, https://doi.org/10.1016/j.watres.2007.04.009.
786 [27] I. Torres, A.K. Marcus, H. Lee, P. Parameswaran, R. Krajmalnik-brown, B.E. Rittmann,
787 A kinetic perspective on extracellular electron transfer by anoderespiring bacteria,
788 FEMS Microbiol. Rev. 34 (2010) 3–17.
789 [28] M.W. Bernardi, M. Dawn, Verbrugge, Mathematical model of a gas diffusion
790 electrode bonded to a polymer electrolyte, AIChE J. 37 (1991) 1151–1163,
791 https://doi.org/10.1002/aic.690370805.
792 [29] M. Karimi Alavijeh, M.M. Mardanpour, S. Yaghmaei, A generalized model for complex
793 wastewater treatment with simultaneous bioenergy production using the microbial
794 electrochemical cell, Electrochim. Acta 167 (2015) 84–96,
795 https://doi.org/10.1016/j.electacta.2015.03.133.
796 [30] O. Wanner, W. Gujer, A multispecies biofilm model, Biotechnol. Bioeng. 28 (1986)
797 314–328.
798 [31] S.B. Velasquez-orta, I.M. Head, T.P. Curtis, K. Scott, J.R. Lloyd, H. Von Canstein, The
799 effect of flavin electron shuttles in microbial fuel cells current production, Appl.
800 Microbiol. Biotechnol. 85 (2010) 1373–1381, https://doi.org/10.1007/s00253-009-
801 2172-8.
802 [32] X. Zhang, A. Halme, Modelling of a microbial fuel cell process, Biotechnol. Lett. 17
803 (1995) 809–814.
804 [33] W. Bae, B.E. Rittmann, A structured model of dual-limitation kinetics, Biotechnol.
805 Bioeng. 49 (1996) 683–689, https://doi.org/10.1002/(SICI)1097-0290(19960320)
806 49:6<683::AID-BIT10>3.0.CO;2-7.
807 [34] M.A. Tsompanas, A. Adamatzky, I. Ieropoulos, N. Phillips, G.C. Sirakoulis, J.
808 Greenman, Modelling microbial fuel cells using lattice Boltzmann methods, IEEE/ACM
809 Trans. Comput. Biol. Bioinforma. 16 (2019) 2035–2045,
810 https://doi.org/10.1109/TCBB.2018.2831223.
811 [35] C.S. Laspidou, B.E. Rittmann, Modeling the development of biofilm density including
812 active bacteria, inert biomass, and extracellular polymeric substances, Water Res. 38

(2004) 3349–3361, https://doi.org/10.1016/j.watres.2004.04.037.

[36] H. Von Canstein, J. Ogawa, S. Shimizu, J.R. Lloyd, Secretion of Flavins by Shewanella species and their role in extracellular electron transfer, Appl. Environ. Microbiol. 74 (2008) 615–623, https://doi.org/10.1128/AEM.01387-07.

[37] E. Marsili, D.B. Baron, I.D. Shikhare, D. Coursolle, J.A. Gralnick, D.R. Bond, Shewanella secretes flavins that mediate extracellular electron transfer, Proc. Natl. Acad. Sci. 105 (2008) 3968–3973.

[38] C.R. Myers, J.M. Myers, Localization of cytochromes to the outer membrane of anaerobically grown Shewanella putrefaciens MR-1, J. Bacteriol. 174 (1992) 3429–3438, https://doi.org/10.1128/jb.174.11.3429-3438.1992.

[39] D.K. Newman, R. Kolter, A role for excreted quinones in extracellular electron transfer, Nature. 405 (2000) 94–97, https://doi.org/10.1038/35011098.

[40] D. Pinto, T. Coradin, C. Laberty-Robert, Effect of anode polarization on biofilm formation and electron transfer in Shewanella oneidensis/graphite felt microbial fuel cells, Bioelectrochemistry 120 (2018) 1–9, https://doi.org/10.1016/j.bioelechem.2017.10.008.

[41] S. Choi, B. Kim, I.S. Chang, Tracking of Shewanella oneidensis MR-1 biofilm formation of a microbial electrochemical system via differential pulse voltammetry, Bioresour. Technol. 254 (2018) 357–361, https://doi.org/10.1016/j.biortech.2018.01.047.

[42] L. Zhang, X. Zhu, J. Li, Q. Liao, D. Ye, Biofilm formation and electricity generation of a microbial fuel cell started up under different external resistances, J. Power Sources 196 (2011) 6029–6035, https://doi.org/10.1016/j.jpowsour.2011.04.013.

[43] N. Uria, I. Ferrera, J. Mas, Electrochemical performance and microbial community profiles in microbial fuel cells in relation to electron transfer mechanisms, BMC Microbiol. 17 (2017), https://doi.org/10.1186/s12866-017-1115-2.